

Study on snowmelt and algal growth in the Antarctic Peninsula using spatial approach

M. Geetha Priya^{1,*}, N. Varshini², G. Chandhana²,
G. Deeksha², K. Supriya² and D. Krishnaveni²

¹School of Electronics Engineering, Vellore Institute of Technology, Chennai 600 127, India

²Centre for Incubation, Innovation, Research and Consultancy and Department of ECE, Jyothy Institute of Technology, Thataguni, Bengaluru 560 082, India

In recent times, global warming across the world is one of the major factors that triggers surface snow melting. According to the reports, climate change across the globe has a major impact on the poles, which has resulted in rapid snowmelt and red-pigmented algal growth. Because of its less sunlight reflecting characteristics, algal growth results in the rapid melting of snow. In this study, we used Landsat images of 30 m resolution to estimate the area of snowmelt and evaluate the impact of algal growth in snow reflectance in Eagle Island, Antarctic Peninsula. Based on the analysis, it is estimated that within a span of 9 days between 4 and 13 February 2020, around 21.37% of the area of snow melted resulting in the formation of a pond of 2.13 km². Variation in the visible band is witnessed, indicating reduction of snow reflectance due to algal growth that leads to reduced albedo and increased warming.

Keywords: Algal growth, climate change, snowmelt, snow reflectance, spatial analysis.

THE Argentine Research Base Esperanza reported that Antarctica measured a temperature of 20.75°C in February 2020, breaking the previous record of 17.9°C observed in March 2015. This extreme temperature was due to heatwave over the Antarctic Peninsula. As a result of extreme pollution of thermal cornering gas, glaciers in Antarctica are melting rapidly¹. According to the World Meteorological Organization, Antarctica ice sheets have enough water to increase the sea level. Due to this extreme high temperature, global sea-level rise may occur at a faster rate².

Eagle Island is one of the climate change-impacted places observed in Antarctica, due to a large amount of snow lost in an interval of nine days. Melt ponds are pools holding saturated water that forms on sea ice in spring and summer. In general, melt ponds are found in Alaska, the Arctic and Greenland^{3–6}. Due to temperature anomaly, melt pond occurrence has been observed in Eagle Island. Another effect of climate change is the formation of red snow near the Vernadsky Research Base

during February 2020 due to algal growth. Scientists from Ukraine have explained that due to red colour, snow reflects less sunlight and melts at a faster rate producing more bright algae⁷.

Red snow was discovered by John Ross in 1818 at Crimson cliff in Baffin's bay near the Arctic region. Later Robert Brown reported that the red colour was caused by algae. At the beginning of the 20th century, Johan Nordal Fischer-Wille proved that the red colour of snow was due to algae that he named *Chlamydomonas nivalis* (photosynthetic green algae)^{8,9}. Green algae grow in snowfields of the Alps and polar regions which consist of red carotenoid pigment that is responsible for the red colour protecting it from UV radiation^{10,11}. The present study is an immediate response to observations on the effect of rise in temperature on snow cover of Eagle Island and the change in snow reflectance due to red algal growth which has been reported by polar researchers in February 2020. This study will help the scientific community to understand the response of snow to anomalous warming by qualitative correlation.

For snow cover and red snow studies, Eagle Island and Galindez Island of the Antarctic Peninsula were chosen (Figures 1 and 2). No other factors can influence these

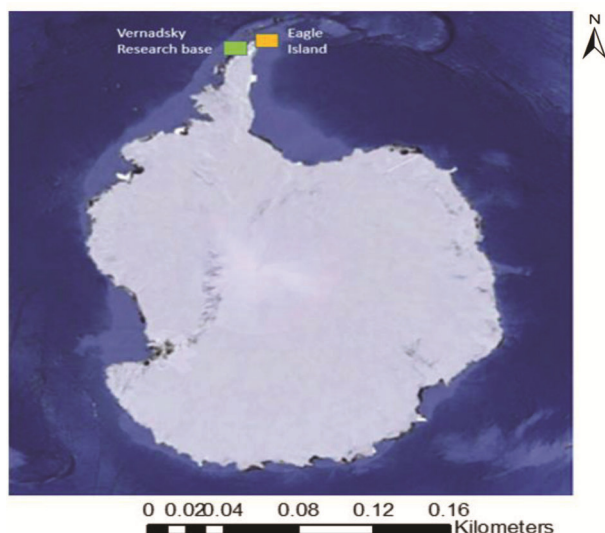


Figure 1. Study area – Antarctic Peninsula.

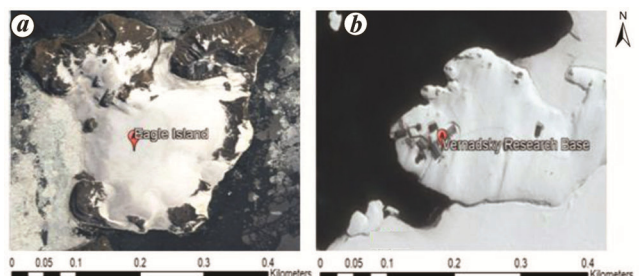


Figure 2. (a) Eagle Island and (b) Vernadsky Research Base.

*For correspondence. (e-mail: geetha.sri82@gmail.com)

Table 1. Data used from LANDSAT-8 Operational Land Imager

Satellite and band used	Study	Date of acquisition	Path no.	Row no.
LANDSAT-8 OLI	Snow cover	4 February 2020	216	104
		13 February 2020	215	105
	Red snow	22 February 2019	219	106
		25 February 2020	219	106

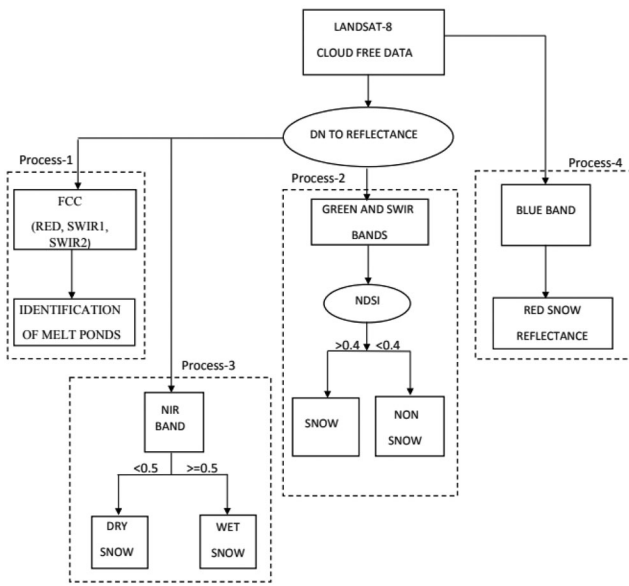


Figure 3. Process flow: (a) Process-1 for melt pond identification, (b) Process-2 for snow cover area mapping, (c) Process-3 for dry/wet snow mapping, and (d) Process-4 for red snow reflectance change.

regions, except temperature anomaly, as other regions of Antarctica are far from tropical countries. Eagle Island ($63^{\circ}39'S$, $57^{\circ}27'W$) is one of several islands around the Peninsula known as Graham Island, which is closer to South America, covering an area of approximately 45 km^2 . It is separated from the Antarctic mainland by the 1.77 km wide Aripleri Passage. The red algal growth was observed around Vernadsky Research Base ($65^{\circ}14'45"S$, $64^{\circ}15'28"W$), which is a Ukrainian Antarctic Station located at Marina Point on Galindez Island of Argentine Islands, not far from Kiev Peninsula. Researchers call the red snow as ‘raspberry snow’ or ‘watermelon snow’.

The multispectral satellite images of LANDSAT-8 OLI downloaded from the United States Geological Survey (USGS) were used for the present study¹². LANDSAT-8 originally known as LANDSAT data continuity mission was launched on 11 February 2013. It is an alliance between NASA and USGS. This satellite provides standard resolution imageries from 15 to 100 m of the earth’s landscape and polar regions. LANDSAT-8 is operated in visible, near-infrared, shortwave infrared and thermal infrared regions¹³. Table 1 presents the details of data used for the present study.

The methodology shown in Figure 3 was adopted to study the climate warming impacts on Eagle Island (estimate the area of snow cover, wet/dry snow mapping and melt pond identification) and the region around Vernadsky Research Base (change in reflectance due to red snow).

The raw data obtained from USGS are available in the form of digital numbers (DN). It is commonly used to describe pixel values that have not yet been calibrated into meaningful physical units. Thus, it is necessary to convert DN to top-of-atmospheric reflectance (TOA) using the eqs (1) and (2) below¹⁴

$$L_{\lambda} = \frac{(L_{\max\lambda} - L_{\min\lambda})DN_{\lambda}}{DN_{\max\lambda}} + L_{\min\lambda}, \quad (1)$$

$$\rho_g = \frac{\pi L_{\lambda} d^2}{E_{\text{sun}\lambda} \cos \theta_s} \times 100, \quad (2)$$

where L_{λ} is the spectral radiance in the band, $L_{\max\lambda}$ the spectral radiance in the band at DN_{\max} , $L_{\min\lambda}$ the spectral radiance in the band at DN_{\min} , DN_{λ} the digital number of pixels in the band, $DN_{\max\lambda}$ the highest DN value in the scale, ρ_g the reflectance in the band, d the Earth–Sun distance (AU), $E_{\text{sun}\lambda}$ the mean solar exoatmospheric spectral irradiance in the band and θ_s is the solar zenith angle.

Melt ponds were identified by means of visual comparison of false colour composite (FCC) images of different temporal resolution. The FCC images using different bands of the electromagnetic spectrum were used to visualize wavelengths that the human eye does not see. The FCC images were composed using red and SWIR-1/2 bands reflectance, showing the existence of melt ponds in Eagle Island on 13 February 2020.

The snow cover area of Eagle Island was mapped using a normalized difference snow index (NDSI) algorithm¹⁵. This involves band ratioing of green and SWIR bands of LANDSAT-8, as given in eq (3). NDSI threshold of 0.4 is applied to distinguish the snow and non-snow regions. The pixels corresponding to values of $NDSI \geq 0.4$ and $NDSI < 0.4$ represent snow and non-snow areas respectively¹⁶

$$NDSI = \frac{\text{GREEN reflectance} - \text{SWIR reflectance}}{\text{GREEN reflectance} + \text{SWIR reflectance}}. \quad (3)$$

Table 2. Percentage of snow cover area (SCA)

Eagle	4 February 2020	13 February 2020
Snow cover w.r.t. total area of Island (%)	90.16	70.89
Dry snow w.r.t. SCA (%)	73.60	17.50
Wet snow w.r.t. SCA (%)	26.15	82.32
Melt Pond w.r.t. SCA (%)	0	6.65

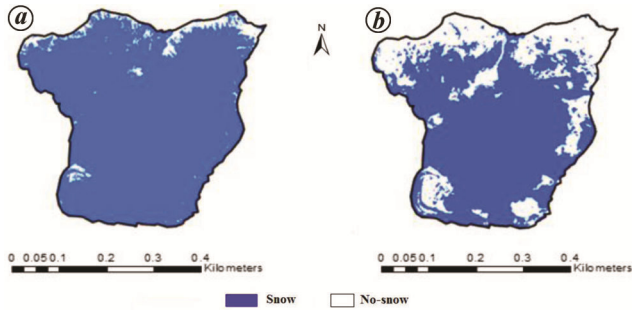


Figure 4. Snow cover area on (a) 4 February 2020 and (b) 13 February 2020.

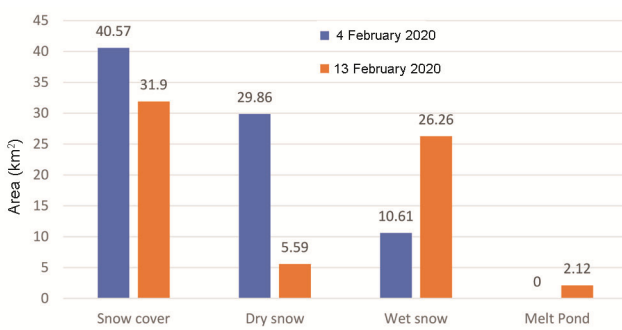


Figure 5. Snow cover area estimated on 4 and 13 February 2020.

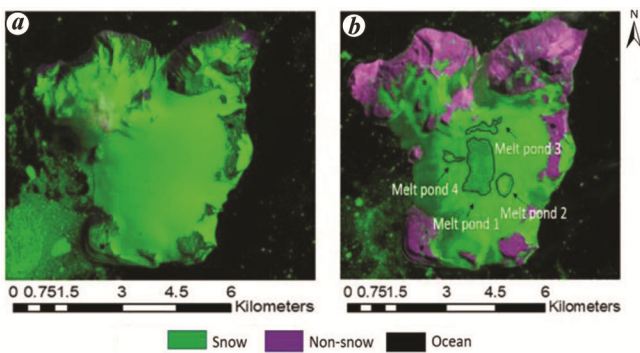


Figure 6. FCC images of (a) 4 February 2020 and (b) 13 February 2020.

The surface melting of snow cover area was identified using the NIR band reflectance thresholding technique¹⁷. Melting snow or wet snow has a lower albedo than freshly fallen or dry snow. This property was used to distinguish between dry and wet snow regions in Eagle Island. Wet snow has a low reflectance in the NIR band due to

the presence of water when compared to dry snow. Thus, a threshold of 0.5 was applied to the NIR reflectance over snow-covered areas, where pixels corresponding to $\text{NIR} \geq 0.5$ were classified as dry snow and the rest as wet snow¹⁷.

Ice and snow have a high albedo and hence high reflectance across all visible wavelengths of the electromagnetic spectrum. Visible bands (red, blue and green) reflectance was considered to study the change in reflectance due to algal growth around Vernadsky Research Base.

Snow cover area estimation, dry/wet snow mapping and delineation of melt ponds in Eagle Island were carried out using Quantum GIS (QGIS v3.12) open-source software. The total area of Eagle Island was estimated to be 45 km². Snow cover map shown in Figure 4, obtained using NDSI thresholding, was used to calculate the area of snow cover on 4 and 13 February 2020. Cloud-free satellite optical data were used to avoid misclassification of cloud pixels as snow pixels during the NDSI process.

Figure 5 and Table 2 show the estimated snow cover area (SCA) and melt ponds due to rapid snowmelt during 4 and 13 February 2020. A snow cover of 40.57 and 31.9 km² was observed on 4 and 13 February 2020 respectively. This is approximately 90.16% and 70.89% respectively when compared to the total area of the Island (Table 2). The area of snow cover lost during this period of nine days was estimated to be around 21.37% due to climate warming. Quantification of snowmelt is beyond the scope of the present study.

NIR reflectance thresholding indicated that wet SCA observed on 4 February 2020 was 26.15%. More than 80% of SCA was wet as on 13 February 2020, which is three-fold more than 4 February 2020. This high percentage of wet snow indicates its rapid melting due to heat-wave and temperature anomaly^{18–20}.

Delineated melt ponds from FCC images showed that four delineated melt ponds with 6.65% of total SCA were observed as 13 February 2020 (Figure 6). The fraction and duration of melt ponds are crucial as they introduce positive feedback into the snow or ice surface by increasing air temperature and reducing the albedo. Figures 7 and 8 show the spectral response of melt ponds in Eagle Island and snow in the RGB spectrum. A comparison reflectance indicates that melt pond has lower reflectance than snow, hence absorbing a large amount of heat from the atmosphere with increase in melting²¹.

Figure 9 shows the spectral response of red snow on 25 February 2020, along a profile drawn around the region

of Vernadsky Research Base in the visible RGB spectrum bands. It is seen that red snow exhibits lesser reflectance in all the visible bands when compared to actual snow. Based on the comparison of snow and red snow reflectance (Figures 8 and 9 respectively), it is observed that the snowfield exhibits a reflectance range 0.36–0.73 in the blue band due to algal growth, which is less compared to the white snow reflectance range. This indicates that the presence of algae in snow affects snow albedo resulting in more warming as well as algal growth.

In this study, spatial analysis has been carried out over Eagle Island and the area around Vernadsky Research Base. The analysis is based on band ratio and LANDSAT-8 OLI data spectral reflectance thresholding. It is observed from the study that approximately 8.67 km² of snow-covered area has melted in a span of nine days,

resulting in the development of four melt ponds measuring 2.12 km² as of 13 February 2020. The presence of less than 20% of dry snow area indicates the state of the island's imbalance with retreating features that, in turn, alert the world. From the growth of algae on snowfields, the reduction in snow albedo and reflectance properties is apparent. Increased warming and further melting would boost algal growth due to a decrease in the reflectance of red snow, providing positive feedback affecting the atmosphere. Methods applied for measuring snow cover and snow reflectance applied to the present study are scientifically well-established and add value to this study. The analysis can be further extended to provide statistics on snow depletion time series with the availability of satellite and temperature data. A useful analysis would be the snow depletion curve for forecasting snowmelt in Antarctica based on the snowmelt factor. Due to all-weather day and night imaging, the use of SAR datasets for such research would also be useful.

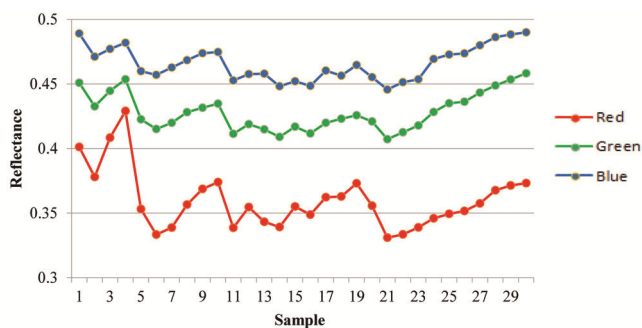


Figure 7. Reflectance from melt pond of Eagle Island.

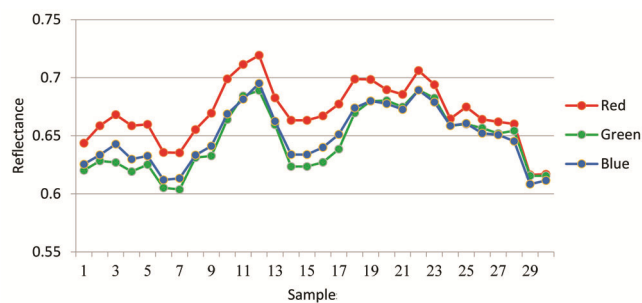


Figure 8. Reflectance of snow around Eagle Island and Vernadsky Research Base.

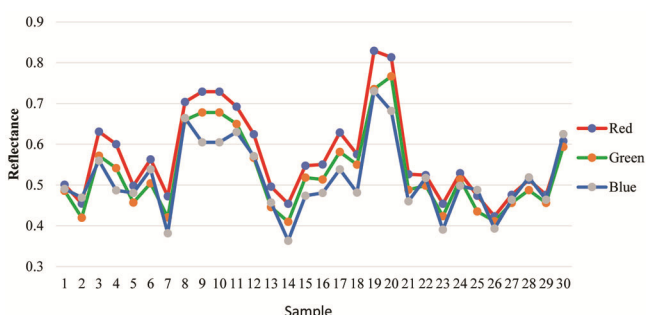


Figure 9. Reflectance of red snow near Vernadsky Research Base.

- Golledge, N. and Jendersie, S., Projecting future sea level rise by coupling models of the Antarctic Ice Sheet, Ice Shelves and the Southern Ocean. *Geophys. Res. Abstr.*, 2019, **21**.
- Matthew J. Hoffman Xylar Asay-Davis Stephen F. Price Jeremy Fyke Mauro Perego, Effect of subshelf melt variability on sea level rise contribution from Thwaites Glacier, Antarctica. *Adv. Earth Space Sci.*, 2019, **124**(12), 2798–2822.
- Turner, J., Summerhayes, C., Sparrow, M. and Mayewski, P., Antarctic climate change and the environment update. *Polar Rec.*, 2016, 509–510.
- Schlosser, E., Haumann, F. A. and Raphael, M. N., Atmospheric influences on the anomalous 2016 Antarctic sea ice decay. *Cryosphere*, 2018, 1103–1119.
- Liu, H. and Wang, L., Spatiotemporal variations of snowmelt in Antarctica derived from satellite scanning multichannel microwave radiometer and Special Sensor Microwave Imager data (1978–2004). *J. Geophys. Res.*, **111**, 1–20.
- M de Los Milagros Skansi, King, J. and Lazzara, M. A., Evaluating the highest temperature extremes in the Antarctic. *Eos*, 2017, 1–6.
- Barkan, J. and Alpert, P., Red snow occurrence in Eastern Europe. A case study. *R. Meteorol. Soc.*, 2020, **75**(2), 1.
- Lutz, S., Anesio, A. M., Edwards, A., Raiswell, R., Newton, R. J., Gill, F. and Benning, L. G., The biogeography of red snow microbiomes and their role in melting arctic glaciers. *Nature Commun.*, 2016, 7.
- Procházková, L., Remias, D., Holzinger, A., Řezanka, T. and Nedbalová, L., Ecophysiological and morphological comparison of two populations of *Chlainomonas* sp. (Chlorophyta) causing red snow on ice-covered lakes in the High Tatras and Austrian Alps. *Eur. J. Phycol.*, 2018, **53**(2), 230–243.
- Daniela, F., Fuentes, R., Huovinen, P. and Gómez, I., Microbial composition and photosynthesis in Antarctic snow algae communities: integrating metabarcoding and pulse amplitude modulation fluorometry. *Algal Res.*, 2020, **45**.
- Tedstone, A. *et al.*, Algal growth and weathering crust state drive variability in western Greenland Ice Sheet ice albedo 2020, **14**(2), 521–538.
- <https://earthexplorer.usgs.gov/>
- Roy, D. P. *et al.*, LANDSAT-8: science and product vision for terrestrial global change research. *Remote Sensing Environ.*, 2014, **145**, 154–172.

14. Markham, B. L. and Barker, J. L., LANDSAT MSS and TM post-calibration dynamic rangers, exoatmospheric reflectance and at-satellite temperatures. *EOSAT LANDSAT Tech. Notes*, 1986, 3–8.
15. Kulkarni, A. V., Srinivasulu, J., Manjul, S. S. and Mathur, P., Field based spectral reflectance studies to develop NDSI method for snow cover monitoring. *J. Indian Soc. Remote Sensing*, 2002, **30**, 73–80.
16. Hall, D. K. and Riggs, G. A., Normalized-difference snow index (NDSI). *Encyclopedia of Snow, Ice and Glaciers*, Springer-Verlag, The Netherlands, 2011, pp. 779–780.
17. Gupta, R. P., Haritashya, U. K. and Singh, P., Mapping dry/wet snow cover in the Indian Himalayas using IRS multispectral imagery. *Remote Sensing Environ.*, 2005, **97**, 458–469.
18. Boris, S., Andrea, M., Jain, S. K., Toby, W. and Ian, H., A method for monthly mapping of wet and dry snow using Sentinel-1 and MODIS: Application to a Himalayan river basin. *Int. J. Appl. Earth Obs. Geoinf.*, 2019, **74**, 222–230.
19. Tsai, Y.-L., Dietz, A., Natascha, O. and Kuenzer, C., Wet and dry snow detection using Sentinel-1 SAR data for mountainous areas with a machine learning technique. *Remote Sensing*, 2019, **11**(8), 895.
20. Antarctica melts under its hottest days on record; <https://earthobservatory.nasa.gov/images/146322/antarctica-melts-under-its-hottest-days-on-record>
21. Flocco, D., Schroeder, D., Feltham, D. L. and Elizabeth, C. H., Impact of melt ponds on Arctic sea ice simulations from 1990 to 2007. *J. Geophys. Res.*, 2012, **117**(C9), 1–17.

Received 30 March 2020; revised accepted 15 January 2021

doi: 10.18520/cs/v120/i5/932-936

Wavelength selection and classification of hyperspectral non-imagery data to discriminate healthy and unhealthy vegetable leaves

Anjana N. Ghule^{1,*} and Ratnadeep R. Deshmukh²

¹Department of Information Technology,
Government College of Engineering, Aurangabad 431 005, India

²Department of Computer Science and Information Technology,
Dr B.A.M. University, Aurangabad 431 005, India

Being the largest vegetarian population across the globe, vegetables are an integral part of Indian meals. The proposed research finds significant wavelengths to discriminate healthy and unhealthy vegetable plants. Spectral-reflectance (SR) and first-derivative (FD) in the visible, red edge and near infrared region (350–1000 nm) of three vegetables brinjal, cluster beans and long beans were used. The significant wavelengths were selected using ReliefF and Support-

Vector-Machine (SVM). Random forest algorithm was used for classification. The binary classification was used for each vegetable separately, and multiclass classification was applied for all the samples. The most significant spectral wavelengths, for the prediction of diseased brinjal, correspond primarily to the red edge in SR. Long beans samples were classified accurately in the red-edge. In the case of cluster beans, SR is more effective than FD in the red-edge. The results substantiate the utility of HS data for discrimination of healthy and unhealthy vegetable plants and even vegetable types.

Keywords: Classification accuracy, healthy and unhealthy vegetable plants, hyperspectral measurements, spectral reflectance, wavelength selection.

HYPERSPECTRAL (HS) data are the spectral reflectance of target objects spread over a large number of narrow and continuous wavelengths over different portions of the electromagnetic spectrum (EMS). Crops exhibit different biophysical and biochemical characteristics like chlorophyll *a* and *b*, total chlorophyll, nitrogen content, carotenoid pigment, anthocyanin, plant stress, plant moisture and cell structure. HS remote sensing has the potential to detect subtle variations in these characteristics, which provide significant information about plant health, plant stress, crop yield and availability of nutrients. Analytical Spectral Devices, Inc. (ASD) spectroradiometer records reflectance spectra ranging from 350 to –2500 nm, covering the visible (Vis), near infrared (NIR) and shortwave infrared (SWIR) regions of the EMS help in the study and analysis of crops. A large number of bands ultimately result in multicollinearity and high correlation along many adjacent wavelengths^{1–3}. The selection of significant spectral region and optimal wavelengths can alleviate the dimensionality, and reduce classification complexity and improve classification accuracy^{4–6}.

For the classification of peatland vegetation, random forest, support vector machine (SVM), regularized logistic regression and partial least square-discriminant analysis (PLS-DA) have been employed, where non-imagery HS data were used⁷. PLSR and linear discriminant analysis (LDA) methods are employed to find the most significant wavebands for discrimination of similar weeds and different species of crops. Diago *et al.*⁸ captured HS images of three types of grapevines leaves for species discrimination. Images were captured using a camera and leaf reflectance was measured over 1040 wavelengths. Almost 92% classification accuracy was obtained by PLS classifier. Zapolkska *et al.*⁹ applied LDA, PLS regression and principal component regression (PCR) to find optimal wavelengths for discrimination between healthy and diseased *Olea europaea* L.

Researchers have used analysis of variance (ANOVA) for selecting optimal spectral bands from both spectral reflectance (SR) and first derivative (FD) for differentiating

*For correspondence. (e-mail: anjanaghule@gmail.com)